On the General Circulation over Eastern Asia (III)

Staff Members of the Section of Synoptic and Dynamic Meteorology, Institute of Geophysics and Meteorology, Academia Sinica, Peking

(Manuscript received October 24, 1957)

Abstract

The averaged vertical motion and the heat sources and sinks have been computed for the normal maps for January and July. The perturbations in the westerlies due to large-scale heat sources and sinks and to the earth's topography are discussed, first using the theory of small perturbations and secondly allowing the perturbations to be of a finite amplitude.

Section 2 contains a discussion of the dynamic influence of the topography on the daily weather systems.

III. Dynamical studies on the general circulation over Eastern Asia

In the first two parts★ (STAFF MEMBERS, 1957, 1958), we have presented the principal results of the synoptic and aerological studies on the general circulation over Eastern Asia. Here in the third part we are going to summarize the dynamical studies. In the dynamical investigations we are primarily concerned with the formation of the mean winter upper air flow pattern and the dynamical influences of the large-scale topography on the daily weather systems over Eastern Asia.

1. The formation of mean winter flow pattern over Eastern Asia

In general there are two extreme views about the cause of formation of the mean upper air circulation. One school emphasizes the thermal origin while the other stresses the dynamical or topographical origin. Here we shall discuss the dynamics of formation of the mean upper air flow over the Far East from a combined view-point.

The large-scale topography over the northern hemisphere is already well-known. However, the distribution of heat sources and sinks is not yet clear. Different authors computed it in different ways. Therefore their results are not at all comparable. Here we have adopted the following three ways for computation:

a. Taking mean of the thermodynamic equation in the steady state, we have

$$Q_m = \frac{gc_p}{R}\frac{1}{\ln p_0/\overline{p}}\left[\mathbf{v}_m \cdot \nabla h - \frac{R\Gamma_p}{g}\ln\left(\frac{p_0}{\overline{p}}\right)\omega_m\right]. \quad (1)$$

Here h is the 1,000—500 mb thickness; $\omega \equiv dp/dt$; $\Gamma \equiv \frac{\gamma_d}{g_\varrho} - \frac{\partial T}{\partial p}$, used as constant; γ_d is the dry adiabatic lapse rate and Q, defined as the heat source (if positive) or sink (if negative), is the rate of heat gained or lost per unit mass and unit time through radiation, turbulence, condensation and evaporation. The remaining symbols are used as usual. Further the subscript "m" represents the mean for 1,000—500 mb; "bar", the value on 500 mb; and subscript "0", values on 1,000 mb or the surface.

★ Hereafter these references will be referred as (I).

The first term on the right of (1) may be calculated from the mean charts of 1,000—500 mb thickness and 700 mb by the geostrophic approximation, $\mathbf{v}_m$ being taken as the wind on 700 mb.

Assuming ω to be a linear function of p, ω_m may then be computed from ω_0 (due to the earth's topography) and $\bar{\omega}$ which in turn may be evaluated from the divergence at 1,000 mb and 500 mb and ω_0. The divergence at 1,000 mb is obtained from the mean surface vector wind, while that on 500 mb is computed as follows: By introducing the vertically-integrated wind components.

$$\bar{u} = \frac{1}{p_0}\int_0^\infty g\varrho u dz,\ \bar{v} = \frac{1}{p_0}\int_0^\infty g\varrho v dz$$

in the tendency equation in the steady state, we get

$$\frac{\partial \bar{u}}{\partial x} + \frac{\partial \bar{v}}{\partial y} = -\frac{1}{p_0}\left(\bar{u}\frac{\partial p_0}{\partial x} + \bar{v}\frac{\partial p_0}{\partial y}\right) + \frac{g}{RT_0} w_0 \quad (2)$$

Here $w_0 = \mathbf{v}_0 \cdot \nabla \eta(x, y)$, $\eta(x, y)$ being the topography of the earth's surface. The expression on the left of (2) may be considered as divergence on 500 mb. $\bar{u}$ and $\bar{v}$ on the right of (2) are taken as the geostrophic wind on 500 mb. Thus the last term of (1) may be calculated.

b. The vertical motion is computed from the divergence of actual wind observations. Advection is also calculated from wind data under the geostrophic assumption. The result of heating obtained from these two terms is checked against radiation (short and long wave) and turbulence.

c. Adopting SAWYER and BUSHBY's (1953) two-parameter model for numerical integration we have

$$\bar{\mathbf{v}} \cdot \nabla (\bar{\zeta} + f) + \frac{1}{3}\mathbf{v}_T \cdot \nabla \zeta_T = \frac{8}{3}\frac{\bar{\omega}\zeta_T}{p_0 - p_1}.$$

Here $\bar{\mathbf{v}}$ and $\bar{\zeta}$ are respectively the geostrophic wind and relative vorticity at the mean level; $\mathbf{v}_T$ and ζ_T, respectively the thermal wind and thermal relative vorticity and f, the Coriolis parameter. In obtaining the above equation the boundary conditions $\omega = 0$ at $p = p_0$ and $p = p_1$ are used. In the same model equation (1) may be written as

$$Q_m = c_p \bar{\mathbf{v}} \cdot \nabla T_0 - \frac{2}{3}\Gamma\bar{\omega}.$$

Eliminating ω from the above two equations we get

$$Q_m = c_p \mathbf{v} \cdot \nabla T_0 - \frac{\Gamma}{4}\frac{p_0 - p_1}{\zeta_T}\left[\bar{\mathbf{v}} \cdot \nabla (\bar{\zeta} + f) + \frac{1}{3}\mathbf{v}_T \cdot \nabla \zeta_T\right], \quad (3)$$

where $\Gamma = \frac{\gamma_a - \gamma_d}{\gamma_d \cdot \varrho}$ assumed to be independent of height.

We have calculated the heat sources by the first method over the northern hemisphere for January and July, by the second method over the Tibetan Plateau and its surroundings for winter and summer and by the third method for northern Asia for winter. The first and second methods give practically the same results while the third method gives similar distribution but too high intensity. We shall give the results by the first method.

The average vertical motion in the lower half atmosphere over the northern hemisphere is shown in fig. 1a (January) and 1b (July). Fixing our attention to Asia and its adjacent regions we see that in winter (fig. 1a) downward motion prevails almost over the whole Asia and Western Pacific which is due to the outbreak of cold air. In summer (fig. 1b) upward motion is present over almost the whole Eurasia with a center over the Tibetan Plateau.

Multiplying ω_m by $c_p\Gamma_p$ we obtain the part of the heat source or sink balanced by vertical motion. This part which is of the same order of magnitude as that part balanced by temperature advection is usually neglected in the computation of heat sources. The distribution of total heat source is shown in fig. 2a (January) and fig. 2b (July). Again fixing our attention to Asia and its adjacent regions we find that in winter (fig. 2a) a cold source is present over the greatest part of Asia and the heat source is centered over the Western Pacific. In summer (fig. 2b) the distribution is almost reversed.

In the following we shall discuss the perturbations on the westerlies due to the large-scale heat sources and sinks and the earth's topography. Using again Sawyer and Bushby's

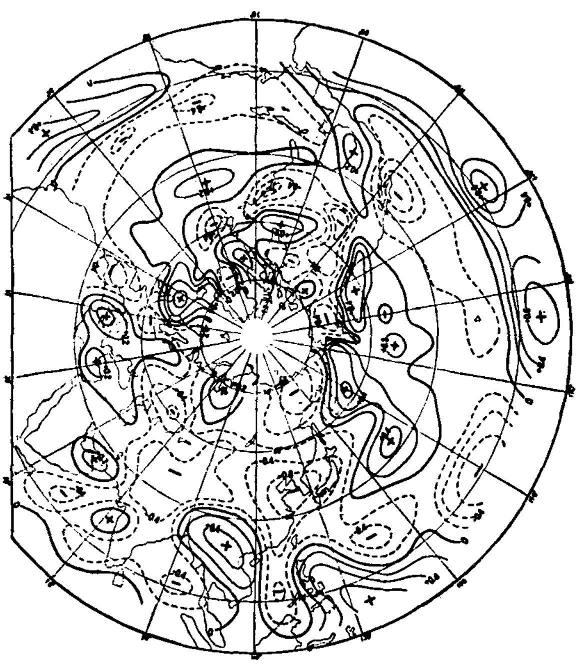

a b

Fig. 1. Mean vertical motion in the lower half atmosphere over the northern hemisphere. (a) January and (b) July (unit: cm sec^{-1}).

a b

Fig. 2. Distribution of heat sources and sinks in the lower half atmosphere over the northern hemisphere (a) January and (b) July (unit: 10^{-5} cal gm^{-1} sec^{-1}).

model we obtain the vertically integrated vorticity equation for the steady state:

$$\overline{\mathbf{v}} \cdot \nabla(f+\overline{\zeta}) + \frac{1}{3}\mathbf{v}_T \cdot \nabla \zeta_T = -\frac{f}{H}\mathbf{v}_0 \cdot \nabla\eta, \quad (4)$$

where $H = RT_0/g$ is the height of the homogeneous atmosphere. In deriving equation (4) the lower boundary condition

$$-\frac{1}{\varrho_0 g}\omega_0 = w_0 = \mathbf{v}_0 \cdot \nabla\eta \qquad \text{at } p = p_0$$

is used. Introducing the assumptions that

$$\mathbf{v}(x, y, p) = \overline{\mathbf{v}}(x, y) + A(p)\,\mathbf{v}_T(x, y),$$
$$\omega(x, y, p) = B(p)\,\overline{\omega}(x, y) + C(p)\,\omega_0(x, y),$$

where $A(p) = (p_0 + p_1 - 2p)/(p_0 - p_1)$, $B(p) = 1 - A^2$ and $C(p) = \frac{p - p_1}{p_0 - p_1}$ ($p_0 = 1{,}000$ mb, $p_1 = 200$ mb), into the steady state vorticity equation, multiplying with $A(p)$, and then integrating it with respect to p from p_0 to p_1, we find

$$\overline{\mathbf{v}} \cdot \nabla\zeta_T + \mathbf{v}_T \cdot \nabla(f + \overline{\zeta}) = \frac{4f}{p_0 - p_1}\overline{\omega}, \quad (5)$$

Again using the assumptions for the distribution of $\mathbf{v}$ (x, y, p) and ω (x, y, p) and the geostrophic approximations in the thermodynamic equation in steady state and eliminating $\overline{\omega}$ from it with equation (5), we have

$$\overline{\mathbf{v}} \cdot \nabla\zeta_T + \mathbf{v}_T \cdot \nabla(f + \overline{\zeta}) = -\frac{Mg}{f}[c_1 Q_m - \overline{\mathbf{v}} \cdot \nabla h], \quad (6)$$

where $c_1 = \frac{R}{gc_p}\ln\frac{p_0}{p}$, $M = \frac{4f^2}{p_0 - p_1}\frac{1}{c_2 R\Gamma_p}$ and $c_2 = \frac{1}{2}\frac{p_0 + 3p_1}{p_0 - p_1} - \frac{4p_0 p_1}{(p_0 - p_1)^2}\ln\frac{2p_0}{p_0 + p_1}$. By introducing perturbation quantities and geostrophic approximation in equations (4) and (6) we obtain the two required differential equations in h and z, where z is the 500 mb perturbation height:

$$\overline{U}\nabla^2 z + \frac{\overline{U}_T}{3}\nabla^2 h + \beta\frac{\partial z}{\partial x} = -\frac{f^2}{gH}(\overline{U} - \overline{U}_T)\,\eta \quad (7)$$

$$\overline{U}\nabla^2\frac{\partial h}{\partial x} + \overline{U}_T\nabla^2\frac{\partial z}{\partial x} + \overline{U}\left(\frac{\beta}{\overline{U}} - M\right)\frac{\partial h}{\partial x} + M\overline{U}_T\frac{\partial z}{\partial x} = -Mc_1 Q_m, \quad (8)$$

where $\nabla^2 = \frac{\partial^2}{\partial x^2} + \frac{\partial^2}{\partial y^2}$ and $\beta = df/dy$. For simplicity the prime sign in the above equations is dropped. In these equations $\overline{U}$ is the speed of the basic current on 500 mb level and $\overline{U}_T$, the thermal wind in 1,000—500 mb layer.

Applying now the above differential equation to a rectangular region with a marginal cyclicity and a length equal to that of the latitudinal circle at 45°, the solution for z may then be written as

$$z(x, y) = \frac{f^2}{gH}\frac{3\overline{U}(\overline{U} - \overline{U}_T)}{3\overline{U}^2 - \overline{U}_T^2}\int_0^{2\pi}\int_0^{2\pi}\eta(\alpha, \nu)\,\phi_\eta(x - \alpha, y - \gamma)\,d\alpha d\gamma + Mc_1\frac{\overline{U}_T}{3\overline{U}^2 - \overline{U}_T^2}\int_0^{2\pi}\int_0^{2\pi} Q_m(\alpha, \nu)\,\phi_q(x - \alpha, y - \gamma)\,d\alpha d\gamma \quad (9)$$

where the topographical influence function ϕ_η and the heating influence function ϕ_q are respectively given by

$$\phi_\eta(x, y) = \frac{1}{4\pi^2}\sum_{\lambda, k = -\infty}^{\infty}\sum \frac{M - \frac{\beta}{\overline{U}} + \lambda^2 + k^2}{\left[(\lambda^2 + k^2)^2 + 2M(\lambda^2 + k^2) - \frac{3M}{2}\frac{\beta}{\overline{U}}\right]}e^{i(\lambda x + ky)}, \quad (10)$$

$$\phi_q(x, y) = \frac{1}{4\pi^2}\sum_{\lambda, k = -\infty}^{\infty}\sum \frac{i(\lambda^2 + k^2)}{\lambda\left[(\lambda^2 + k^2)^2 + 2M(\lambda^2 + k^2) - \frac{3M}{2}\frac{\beta}{\overline{U}}\right]}e^{i(\lambda x + ky)}. \quad (11)$$

These series may easily be transformed into other forms which converge very rapidly.

With a time unit of one day and a length unit of the radius of 45° latitude circle we use for the winter case $\overline{U} = 0.287$, $\overline{U}_T = 0.245$ (corresponding $\overline{U} = 15$ m/s, $\overline{U}_T = 13$ m/s) $M = 231$ and $\beta/\overline{U} = 21.9$. Fig. 3a is the 500 mb flow pattern due to topographical effect only ($Q_m = 0$). In this figure we see that the position of the major trough and ridge is correctly presented. But the intensity of the southern part of the trough and ridge is much stronger than in the actual case. Further the band of

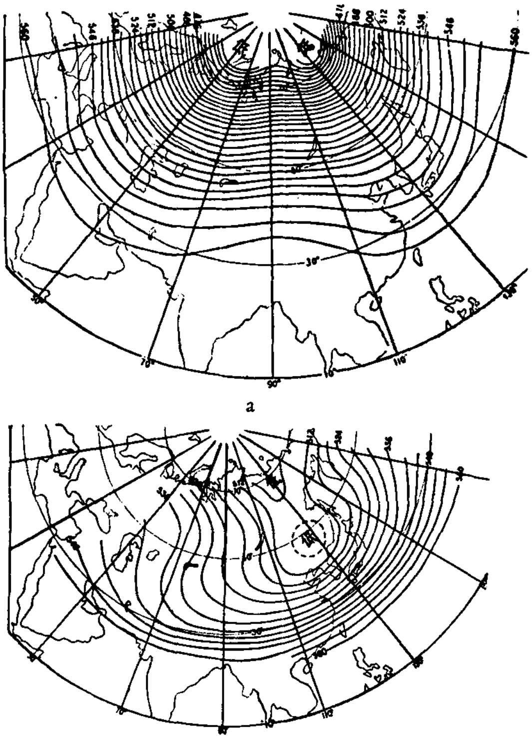

Fig. 3. Steady 500 mb flow pattern produced by the effect of (a) Tibetan Plateau and its adjacent mountains and (b) heat sources and sinks in the westerlies.

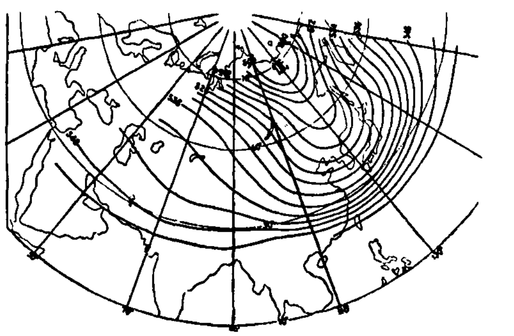

Fig. 4. Steady 500 mb flow pattern produced by the combined effect of mountains and heat sources and sinks in the westerlies.

strong westerlies is too much to the north of the observed position. Fig. 3b is the 500 mb topography due to large-scale heating only ($\eta=0$). This figure also gives a correct position of the Asiatic major trough, but the ridge over Tibet and its adjacent plateau does not appear. The overall pattern of fig. 3a is better (i.e. nearer to the observed one) than that of fig. 3b. But in fig. 3b the strong Asiatic Jet is correctly shown. The combined effect of topography and large-scale heating on the flow pattern over the Far East is presented in fig. 4. Comparing this figure with fig. 1 of (I) we find that the computed trough and ridge as well as the jet check with the observed one fairly well.

The above investigation is based on small perturbation theory. To go one step further we attempted to discuss the dynamics of topographically produced perturbations of finite amplitude in a three-dimensional baroclinic current. Eliminating ω between the steady state vorticity equation and the thermodynamic equation in spherical coordinates (λ, Θ, p) we find

$$J\left(\frac{\nabla^2\phi}{f}+\frac{f}{\sigma}\frac{\partial^2\phi}{\partial p^2}+2\Omega\cos\Theta,\phi\right)=0 \quad (12)$$

where $J(A, B)\equiv\dfrac{\partial A}{\partial q}\dfrac{\partial B}{\partial\lambda}-\dfrac{\partial A}{\partial\lambda}\dfrac{\partial B}{\partial q}$, $q=\cos\Theta$;

$$\nabla^2\equiv\frac{1}{R^2\sin\Theta}\left[\frac{\partial}{\partial\Theta}\left(\sin\Theta\frac{\partial}{\partial\Theta}\right)+\frac{1}{\sin\Theta}\frac{\partial^2}{\partial\lambda^2}\right];$$

λ is the longitude; Θ, the co-latitude; R, the earth's radius; Ω, angular speed of the earth's rotation; $\sigma\equiv-\dfrac{1}{\varrho}\dfrac{\partial\ln\Theta}{\partial p}$, the static stability factor assumed to be constant; and ϕ, the geopotential. The general solution of equation (12) is

$$\frac{\nabla^2\phi}{f}+\frac{f}{\sigma}\frac{\partial^2\phi}{\partial p^2}+2\,\Omega\cos\Theta=F(\phi) \quad (13)$$

where $F(\phi)$ is an arbitrary function of ϕ. Under the assumption that the perturbation ϕ' vanishes in the vicinity of the poles and that the angular speed of the basic current is only a linear function of p, $F(\phi)$ may be determined as

$$F(\phi)=-\frac{2(\bar{\dot\lambda}+\Omega)}{fR^2\bar{\dot\lambda}}\phi. \quad (14)$$

Neglecting $\bar{\dot\lambda}$ against Ω we finally obtain a differential equation for a finite perturbation ϕ'

$$\frac{\partial^2\phi'}{\partial P^2}+\frac{1}{R^2\sin\phi}\left[\frac{\partial}{\partial\Theta}\sin\Theta\frac{\partial\phi'}{\partial\Theta}+\frac{1}{\sin\Theta}\frac{\partial^2\phi'}{\partial\lambda^2}\right]+$$
$$+\frac{2\Omega}{R^2\bar{\dot\lambda}}\phi'=0. \qquad \left(P=\frac{\sqrt{\sigma}}{f}p\right) \quad (15)$$

The upper boundary condition is taken as

$$\phi' = 0 \text{ at } p = 0. \qquad (16)$$

The lower boundary condition may be formed from the thermodynamic equation which on the earth's surface $p = p_0\ (\lambda, \Theta)$ is written as

$$J\left(\frac{\partial \phi}{\partial p}, \phi\right)\Bigg|_{p=p_0} = f R^2 \sigma \varrho_0 g w_0,$$

$$w_0 = \frac{1}{R^2 f} J\,(\eta, \phi_0) \qquad (17)$$

where the geostrophic assumption is used.

Neglecting the variation of ϱ_0, the general solution of equation (17) is:

$$\frac{\partial \phi}{\partial p}\bigg|_{p=p_0} - \sigma \varrho_0 g \eta = G\,(\phi_0) \qquad (18)$$

where $G(\phi_0)$ is an arbitrary function of ϕ_0 which may similarly be found as $F(\phi)$ in the following form

$$G\,(\phi_0) = -\frac{\bar{\lambda}_p}{\bar{\lambda}_0}\phi_0 \qquad \left(\bar{\lambda}_p = -\frac{d\bar{\lambda}}{dp} > 0\right)$$

Finally the lower boundary condition is obtained as

$$\frac{\partial \phi'}{\partial P} + c\,\phi' = H\,(\lambda, \Theta) \quad \text{at } P = P_0\,(\lambda, \Theta) \qquad (19)$$

where $c = f\bar{\lambda}_p / \sqrt{\sigma}\,\bar{\lambda}_0$, $H\,(\lambda, \Theta) = f\varrho_0 g\sqrt{\sigma}\,\eta(\lambda, \Theta)$.

The differential equation (15) is to be solved under the boundary conditions (16) and (19). It gives

$$\phi'\,(\lambda, \Theta, p) = f \varrho_0 g \sqrt{\sigma} \sum_{n=1}^{\infty} \sum_{m=1}^{n} \frac{e^{-\frac{1}{2}(\xi - \xi_0)}\,[\psi_1\,(\xi_1)\,\psi_2\,(\xi) - \psi_2\,(\xi_1)\,\psi_1\,(\xi)]}{2\,k\triangle} \times$$

$$[h_n^m \cos m\lambda + h'^m_n \sin m\lambda]\,P_n^m\,(\cos \Theta) \qquad (20)$$

$$\text{where } \xi = \frac{2k\sqrt{\sigma}}{f\bar{\lambda}_p}\left[\bar{\lambda}_0 + \bar{\lambda}_p \frac{f}{\sqrt{\sigma}}(P_0 - P)\right],$$

$$\xi_0 = \frac{2k\sqrt{\sigma}\,\bar{\lambda}_0}{f\bar{\lambda}_p}, \quad \xi_1 = \frac{2k\sqrt{\sigma}}{f\bar{\lambda}_p}\left(\bar{\lambda}_0 + \bar{\lambda}_p \frac{f}{\sqrt{\sigma}} P_0\right)$$

$P_n^m\,(\cos \Theta)$ is the associated Legendre function and h_n^m and h'^m_n are coefficients of the spherical harmonic series expressed for the mountain function $\eta(\lambda, \Theta)$. ψ_1 and ψ_2 are the two fundamental solutions of the confluent hypergeometric equation

$$\frac{d^2\psi}{d\xi^2} - \frac{d\psi}{d\xi} + \frac{r}{\xi}\psi = 0, \quad \text{where } r = \Omega / kR^2\bar{\lambda}_p \frac{f}{\sqrt{\sigma}}$$

They are given by CHARNEY (1947).

$$\psi_1 = \frac{\sin \pi a}{\pi}\left\{a\,\xi\,M\,(a+1, 2, \xi) \times \left[\ln \xi + \frac{\Gamma'(a)}{\Gamma(a)} - 2\frac{\Gamma'(1)}{\Gamma(1)}\right] + 1 + \sum_{n=1}^{\infty} Bn \frac{a\,(a+1) \cdots (a+n-1)}{(n-1)!\,n!}\xi^n\right\},$$

and $\psi_2 = \xi M\,(a+1, 2, \xi)$. Here $a = -r$, $B_n = \sum_{\nu=0}^{n-1}\left(\frac{1}{a+\nu} - \frac{2}{1+\nu}\right) + \frac{1}{n}$, $M\,(a, b, \xi) = 1 + \frac{a}{1 \cdot b}\xi + \frac{a\,(a+1)}{2!\,b\,(b+1)}\xi^2 + \cdots$, and $\Gamma(a)$ is the Gamma function.

Numerical computation is carried out with $\sqrt{\sigma} = 0.128$ m mb^{-1} sec^{-1}, $\bar{\lambda}_0 = 0.63 \times 10^{-6}$ sec^{-1}, and $\bar{\lambda}_p = 0.68 \times 10^{-8}$ sec^{-1} mb^{-1}. With these constants the series $\psi_1(\xi)$ and $\psi_2(\xi)$ computed by CHARNEY (1947) may be used. The flow over the northern hemisphere on 850 mb, 700 mb, 500 mb and 300 mb is computed. Fig. 5 is the 700 mb topography. From this figure we see that the position of the major troughs and ridges over the eastern world is in good agreement with observation, but there is a discrepancy between the computed and observed intensity of these systems. As in the theory of small perturbation the intensity of the computed troughs and ridges is too strong to the south.

The computed flow pattern over the western world is not in good agreement with the observed. It is because the flow over North America without friction is too much influenced by the Tibetan Plateau which has

$$\triangle = \begin{vmatrix} \left[\frac{d\psi_1}{d\xi} - \left(\frac{1}{2} + \frac{c}{2k}\right)\psi_1\right]_{\xi=\xi_0} & \left[\frac{d\psi_2}{d\xi} - \left(\frac{1}{2} + \frac{c}{2k}\right)\psi_2\right]_{\xi=\xi_0} \\ \psi_1\,(\xi_1) & \psi_2\,(\xi_1) \end{vmatrix}, \text{ and } k^2 = \frac{n\,(n+1)}{R^2}$$

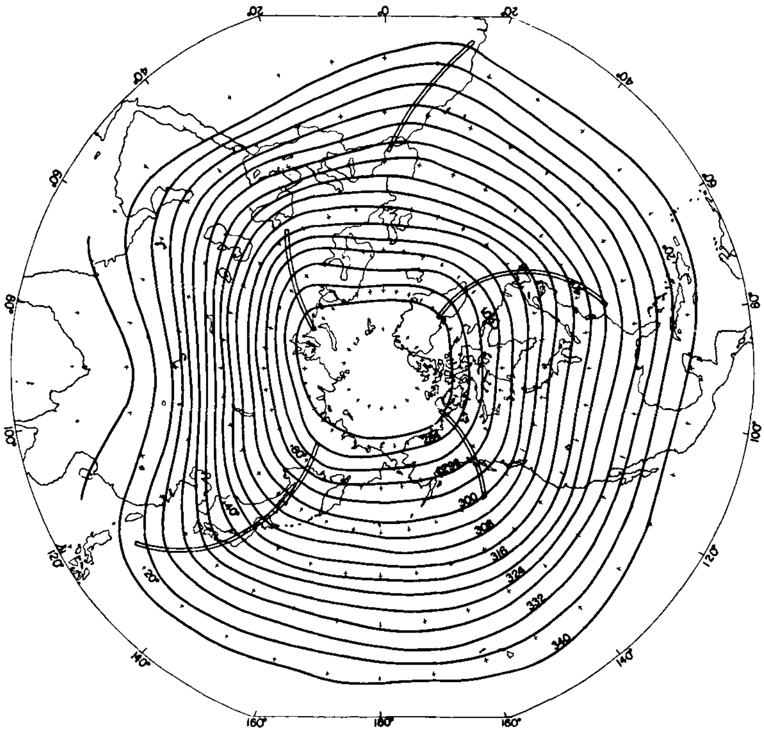

Fig. 5. 700 mb flow pattern produced by the earth's topography over the northern hemisphere.

much larger dimension than the Rocky Mountains. Considering these mountains alone the computed flow (figure not presented) over North America is in better agreement with the actual one.

It is also worth to point out that the axes of the computed troughs and ridges are vertical and the amplitude decreases quickly with increasing height. The former fact may also be shown in the foregoing theory of small perturbation. It is believed that this is due to the neglection of friction.

2. The dynamic influence of the orography on the daily weather systems

In the above we have tried to discuss the dynamics of the formation of mean flow pattern over Asia. Here in this section we shall attempt to discuss the dynamic influence of the orography on the development and movement of the daily weather systems over Eastern Asia and see how far the fact mentioned in (I) can be explained in this way.

In (I) it is pointed out that most of the troughs fill and most of ridges intensify on the wind side of Tienshan-Altai mountain ranges while Lake Baikal is the site for the development of the troughs and weakening of the ridges. These phenomena will be understood from the computations of tendencies due to orographical disturbance in a barotropic model. The vorticity equation in this model may be written as

$$\nabla^2 \frac{\partial z}{\partial t} = J\left(\frac{g}{f}\nabla^2 z + f, z\right) + \frac{f^2}{g\varrho}\frac{\partial \varrho w}{\partial z}. \quad (21)$$

Here the vorticity has been substituted by the geostrophic one. Because of the linearity of the equation with respect to $\frac{\partial z}{\partial t}$, the tendency due to orography may be calculated separately by the following differential equation.

$$\nabla^2 \frac{\partial \bar{z}}{\partial t} = -\frac{f^2}{gH} w_0. \quad (22)$$

Here $\partial \bar{z}/\partial t$ may be considered as the rate of height change of 500 mb surface, $w_0 = \mathbf{v}_0 \cdot \nabla \eta$

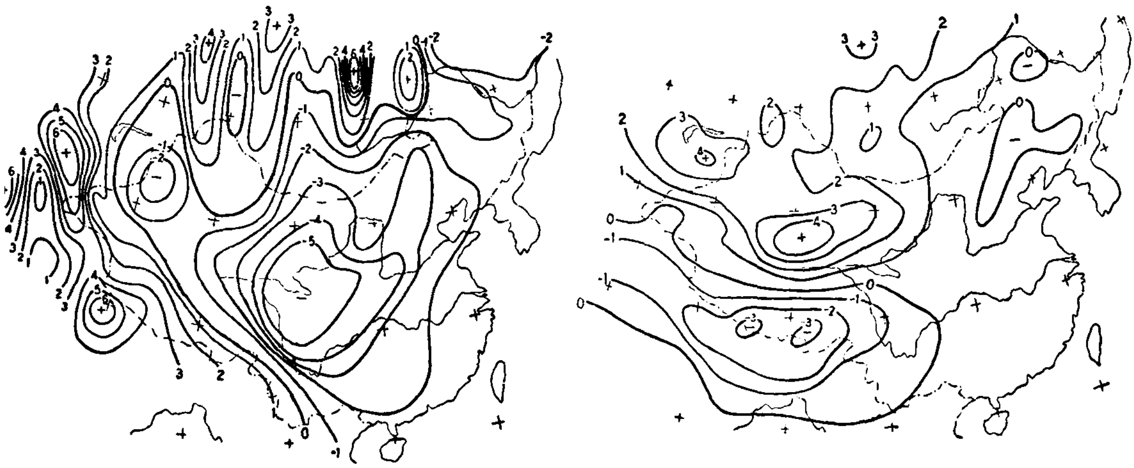

a b

Fig. 6. The barotropic tendency on 500 mb due to orographical disturbance over China (unit: dm/day) (a) with $u_0 = 10$ m/s, $v_0 = 0$, (b) with $v_0 = -5$ m/s, $u_0 = 0$.

and $H = p_0/\varrho_0 g$ is the height of homogenous atmosphere.

The approximate solution (FJØRTOFT, 1952) of the difference equation corresponding to (22) is

$$\frac{\partial \bar{z}}{\partial t} = \frac{d^2}{4gH}\left(\frac{f^2}{m^2} w_0 + 3\left[\frac{f^2}{m^2} w_0\right]\right), \; 4d < \lambda < 8d. \tag{23}$$

Here the brackets represent the mean over the four surrounding grid-points with grid length d, m being the magnification factor of the map projection and λ being the wave length of the motion suitable for the above equation. With a Lambert projection of scale $1 : 2 \times 10^7$ (latitude 30° and 60° being standard parallels) and $d = 2.75$ cm (equal to the length of 5° longitude at along 70° N),

$$\frac{\Delta \bar{z}}{\Delta t} = 1.05 \times 10^{-3}\left(\frac{f^2}{m^2} w_0 + 3\left[\frac{f^2}{m^2} w_0\right]\right) \tag{24}$$

$\Delta \bar{z}/\Delta t$ in unit of 10 geopotential meter per day and the physical quantities on the right of (24) in c.g.s. units.

With (24) and the smoothed topography of Eastern Asia (averaged over 2 degree latitude square) we have computed the tendencies on 500 mb due to orographical disturbance in a westerly current of 10 mps and in a northerly current of 5 mps (fig. 6a, b).

Fig. 6a shows negative tendencies in the regions of Kansu, SW Sinkiang and North China. These are just the regions where the troughs usually develop or form. West of Sinkiang are positive tendencies. These are just the regions where troughs usually fill. Fig. 6b indicates that in a north current there will be positive tendencies over Kansu. Thus during NW current, troughs are not apt to develop or form over this area. This agrees well with our synoptic experience. Further it is to be noted that under the same condition the tendency (positive or negative) computed here is about twice as large as that over the Rockies computed by BOLIN and CHARNEY (1951). Thus the dynamic effect of the plateau over Asia is more pronounced than that of the Rockies.

Because the development of the troughs over North China has special interest for us, we have made a further investigation on it. With $d = 300$ km we have computed by relaxation method the surface tendencies due to orographical disturbances over North China in a barotropic atmosphere in a NW current of 10 mps (fig. 7). The negative tendencies shown in the figure agree quite well in position and magnitude with the development or formation of the 'North China Trough' formed at the beginning of the outbreak of northwesterlies. In general fine weather is associated with this type of troughs (fig. 8). This is different from the situation associated with other types of troughs in this region. This is because this type of trough is formed dynamically in a descending current.

Though we have some success with a barotropic model, yet there are two defects in this model: Firstly in general actual $\mathbf{v}_0$ is much smaller than that used for computation, therefore the computed tendency is much smaller than that observed if actual $\mathbf{v}_0$ is used. Secondly the computed tendency does not change with height in a barotropic model while in actual cases the upper current seems to be less disturbed by the mountain. In a stratified baroclinic atmosphere the result of similar computations will be free from the above defects. Actually the upward decrease of orographical perturbation in this atmosphere has been shown in the foregoing discussion. From the first law of thermodynamics and equation of vorticity we may obtain

$$\nabla^2 \omega + \frac{f^2}{\sigma} \frac{\partial^2 \omega}{\partial p^2} = 0. \qquad (25)$$

Equ. (25) is to be solved under boundary conditions $\omega(p_0) = \omega_0 = -g\varrho_0 \mathbf{v}_0 \cdot \nabla \eta$ and $\omega(0) = 0$. Then from

$$\nabla^2 \frac{\partial z}{\partial t} = \frac{f^2}{g} \frac{\partial \omega}{\partial p} \qquad (26)$$

we may compute $\partial z/\partial t$ at any level.

By this method we calculated the tendency on 300 mb, 500 mb, 700 mb and 900 mb produced by Tienshan-Altai mountain ranges with surface westerlies of 5 mps. η is averaged over 5° latitude square, $\sigma = 2 \times 10^2$ cm^2 sec^{-2} mb^{-2}, horizontal grid length being 390 km and the vertical grid length being 100 mb. Equation (25) has been solved by three-dimensional relaxation method with irregular stars at the boundary.

The results of the computation show that the perturbations produced by the large-scale topography in a stably stratified atmosphere decreases rapidly with height. On the wind side of the Tienshan-Altai mountain ranges the positive tendency at 300 mb is around

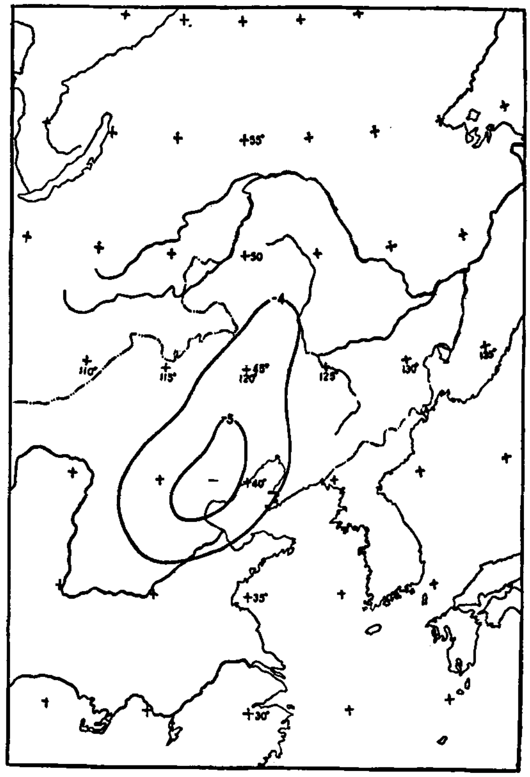

Fig. 7. The barotropic sea level tendency due to orographical disturbance over North China with surface NW wind of 10 m/s (unit: mb/day).

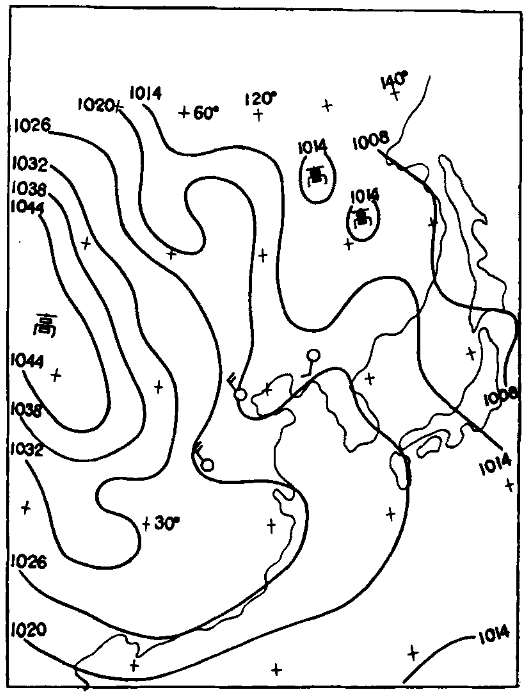

Fig. 8. Typical case of 'North China Trough' (surface chart Jan. 10, 1956, 18 z), notice the clear weather in the trough.

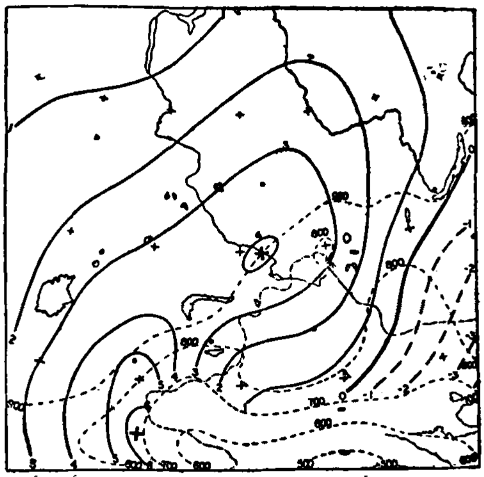

Fig. 9. The 700 mb tendency due to orographical disturbance of Tienshan-Altai mountain ranges in a stratified atmosphere (unit: dm/day). Thick lines: lines of equal tendency, thin dash lines: lines of equal pressure height (in mb) of earth's topography.

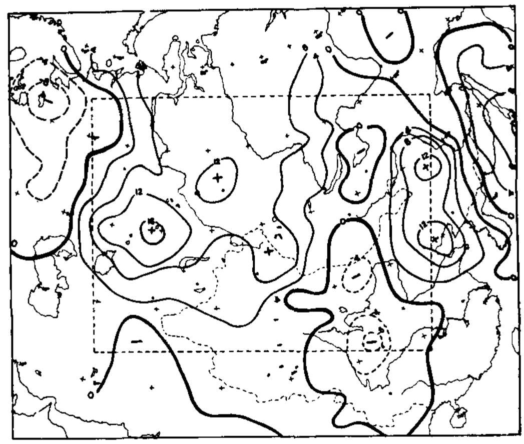

Fig. 11. Observed 24 hr tendency for 700 mb surface in decameters (from Jan. 26 (03 z) to 27 (03) 1957).

20 m/12h, but on 500 mb it is around 30 m/12h, on 700 mb, 40—60 m/12h and on 900 mb it reaches 60—80 m/12h. The distribution on 700 mb is shown as an example in fig. 9

From above it is seen that in the lower troposphere the orographical perturbation in a stratified atmosphere is about 4 times as big as that in a neutral atmosphere under the same condition. Further we may conclude from this that in the forecast of flow pattern in the lower troposphere around the Tibetan Plateau the dynamics of topography must be taken into consideration.

As an illustration of anticyclogenesis on the wind side of Tienshan-Altai mountain ranges we may give the following example. On Janu-

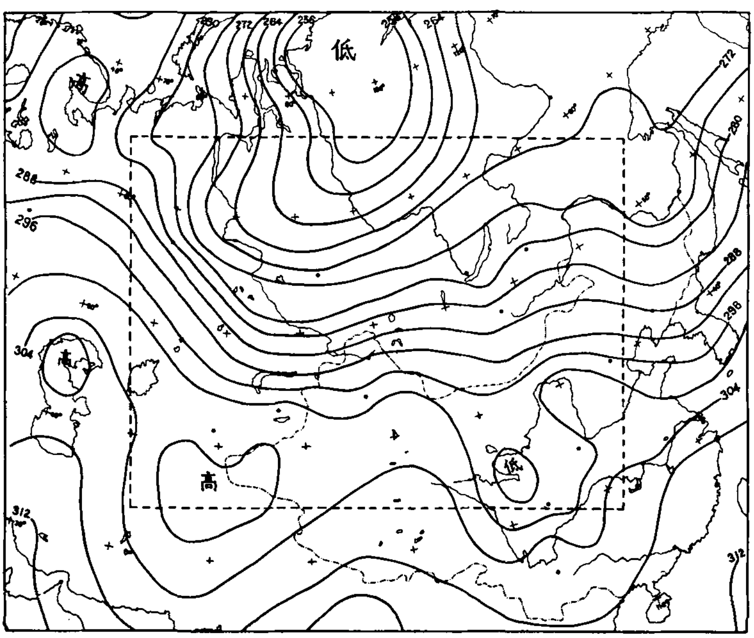

Fig. 10. 700 mb chart, Jan. 26, 1957 (15 z). Isohypes labelled in decameters.

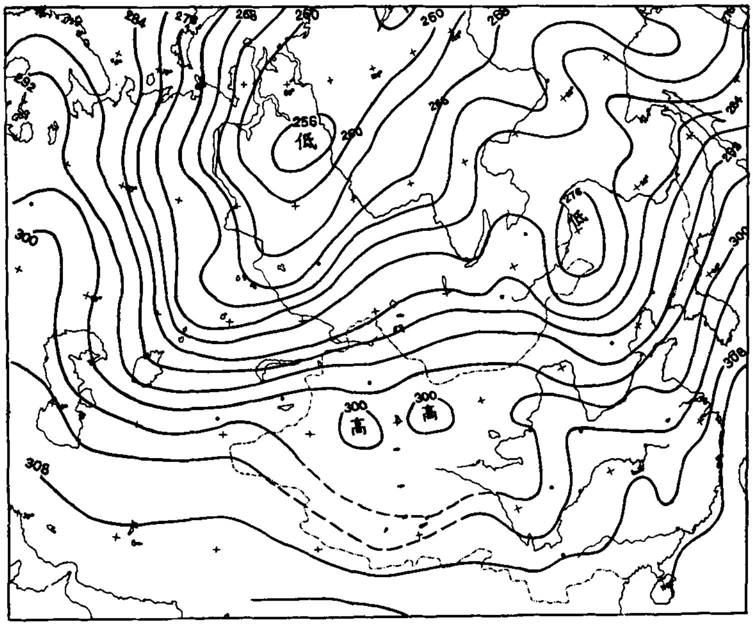

Fig. 12. 700 mb chart Jan. 25, 1957 (15 z).

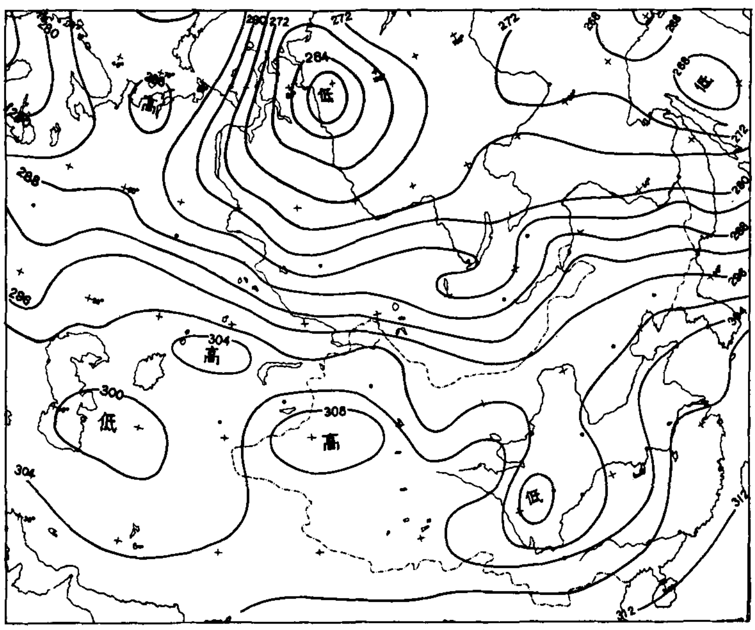

Fig. 13. 700 mb chart Jan. 27, 1957 (15 z).

ary 26, 1957 there is a flat trough on 500 mb (1500 Z) moving to NW China (fig. 10). The observed 24 hour (12 hours before and 12 hours after the map time) height change on 700 mb reaches 80 meters over Balkhask (fig. 11). On the wind side of these mountain ranges we may observe rapid anticyclogenesis on 700 mb (fig. 12—13) and even more clearly on the surface map. Using half of the actually observed geostrophic wind as $\mathbf{v}_0$,

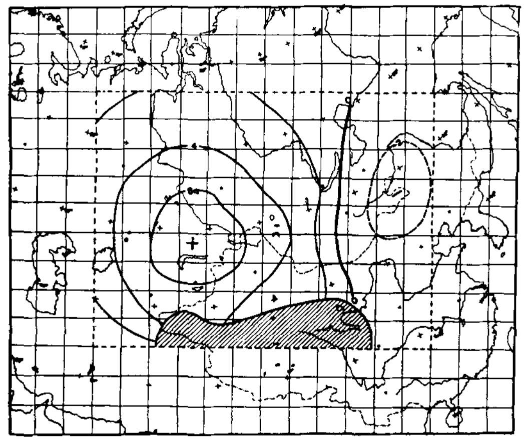

Fig. 14. Calculated tendency for 700 mb surface Jan. 26, 1957 (15 z) due to orographical disturbance, in dm/24 hr. (Shaded area: Plateau with pressure altitude higher than 700 mb.)

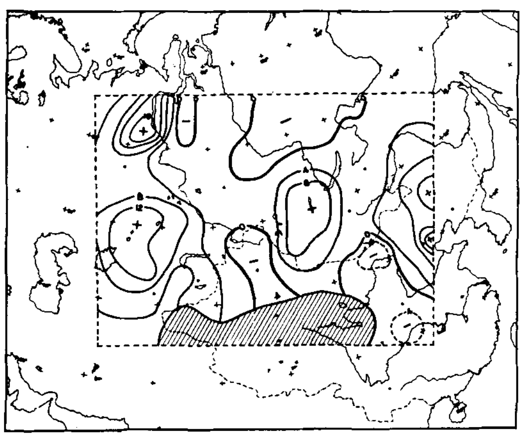

Fig. 15. Computed 24 hr tendency for 700 mb surface.

we computed the tendencies due to orographical disturbances (fig. 14). The maximum tendency reaches 70 m/24 hr. Beside this we also computed the distribution of the tendencies on different levels due to the advection of vorticity and the "free" vertical motion. We find that the distribution of the sum of these two 24 hour tendencies on 700 mb (fig. 15) agrees fairly well with the observed one. It is, however, to be noted that the positive height change associated with low level anticyclogenesis on the wind side of the mountain range is almost entirely contributed by the mountain. Thus the development or genesis of certain anticyclones in this region seems largely due to dynamic effect of orography.

Computation of the rapid filling of the troughs on the wind side of Tienshan-Altai has also been made. The results also show that the computations with consideration of the dynamics of topography check better with observations than that without topography being considered.*

Besides the development the movement of the weather systems may also be influenced by topography. It is our experience that the movement of the weather systems is faster on the north than on the south of Tibetan Plateau though the general steering current is stronger on the south side. It is easy to understand that on the northern (southern) slope prevails horizontal convergence (divergence) associated with the downward motion in the southerly current in front of a trough while there is divergence (convergence) in front of a ridge. Thus under the same general situations the systems would move faster on the northern slope than on the southern slope.

Let us take an ideal mountain $\eta = a\,(1 - |y|/b)$, the origin of y being placed on the mountain ridge. Assuming that ω decreases linearly with p and $\omega(0) = 0$ then $\omega(p) = \omega_\eta \dfrac{p}{p_\eta} \cong - \dfrac{g}{RT_\eta}\dfrac{\partial \eta}{\partial y} v_\eta p$, the subscript η indicating values on the mountain. In small motion the equation of continuity and vorticity equation are respectively

$$\frac{\partial u'}{\partial x} + \frac{\partial v'}{\partial y} = \frac{g}{RT_\eta}\frac{\partial \eta}{\partial y} v_\eta \tag{27}$$

and $$\left(\frac{\partial}{\partial t} + U\frac{\partial}{\partial x}\right)\left(\frac{\partial^2 v'}{\partial x^2} - \frac{\partial^2 u'}{\partial x \partial y}\right) + \frac{\partial v'}{\partial x}\beta = f\frac{\partial}{\partial x}\left(\frac{\partial w}{\partial p}\right) \tag{28}$$

* It may also be of interest to point out that according to our computation for a case (January 15, 1950) the formation of a Vb cyclone may be explained by the dynamic effect of the Alps. In the example used the upper air cut-off low was formed after the surface Vb cyclone. Thus PALMÉN's (1949) mechanism does not account for the formation of a surface Vb cyclone, in this example at least.

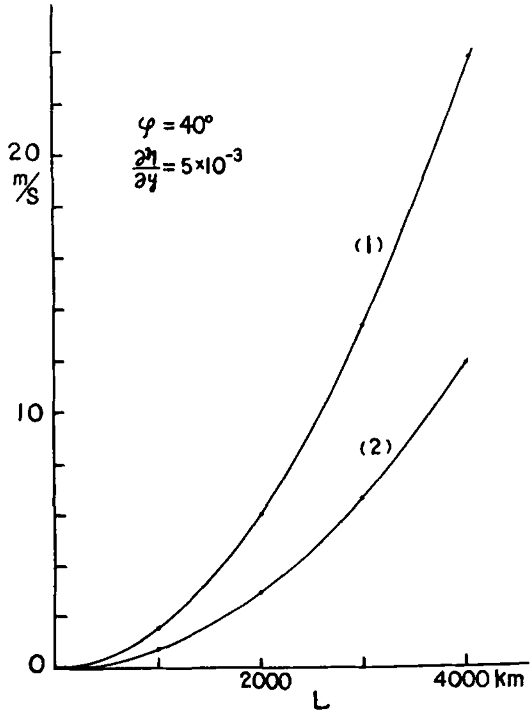

Fig. 16. Change of phase velocity (in m/s) as a function of wave length (in 1,000 km).
[1]) $L = 2\pi/k$, (motion independent of y)
[2]) $L = 2\pi/k = 2\pi/\mu$

Eliminating u' and assuming $v_\eta = v'$ we obtain

$$\left(\frac{\partial}{\partial t} + U\frac{\partial}{\partial x}\right)\left(\frac{\partial^2 v}{\partial x^2} + \frac{\partial^2 v}{\partial y^2} - \alpha\frac{\partial v}{\partial y}\right) + \beta'\frac{\partial v}{\partial x} = 0, \tag{29}$$

the prime on v being dropped and $\beta' = \beta + \alpha f$, $\alpha \equiv \frac{g}{RT_\eta}\frac{\partial \eta}{\partial y}$. Assuming a solution $v \propto e^{i(kx + \mu y - \nu t)}$ we have

$$c = \frac{\nu}{k} = U - \frac{\beta'}{(k^2 + \mu^2)^2 - (\alpha\mu)^2}\left[k^2 + \mu^2 + i\alpha\mu\right]. \tag{30}$$

Assuming the motion to be independent of y, we have

$$c = U - \frac{L^2}{4\pi^2}\left(\beta + \frac{fg}{RT_\eta}\frac{\partial\eta}{\partial y}\right) \tag{31}$$

Evidently

$$C \gtrless U - \frac{\beta U^2}{4\pi^2} \quad \begin{matrix}\text{north slope.}\\ \text{south slope.}\end{matrix}$$

The change of phase velocity due to orography is a function of wave length. Their relation, for $\varphi = 35°$ N and $\partial\eta/\partial y = 4\times10^{-3}$ (roughly equal to the slope of Tibetan Plateau), is given in fig. 16. For $L = 3\times10^8$ cm this velocity reaches several mps.

Concluding remarks

Above we have sketched part of our research work in recent years on the general circulation over Eastern Asia. Through these studies we get a better understanding of the structure, variation and dynamics of the circulation over this part of the world. But we are aware that there are many important synoptic, aerological or dynamic problems we have not touched upon or not even thought of. However, in our next Five Year Plan our pibal and sounding stations become denser and denser and a rawin net is also going to be established. With the observations from this network of stations we would be able to do more work.

This third part of our report is a summary of the following papers:

Chao Jih-ping, 1956: A preliminary study of the distribution of heat source over Eastern Asia in winter computed from the flow pattern. *Acta Meteorologica Sinica*, **27**, 167—180 (in Chinese).

— 1957: On the dynamics of orographically produced finite perturbations in baroclinic westerlies. *Acta Meteorologica Sinica*, **28**, 303—314 (in Chinese).

Chu Pao-chen, 1957: The steady state perturbations of the westerlies by the large-scale heat sources and sinks and earth's orography (I). *Acta Meteorologica Sinica*, **28**, 122—140 and (II) ibid, 198—224 (in Chinese).

— 1957: A note on the orographical effect on the formation of the mean temperature field. *Acta Meteorologica Sinica*, **28**, 315—319 (in Chinese).

Liu Jui-chih and Koo Chen-chao, 1957: On the formation of North China Trough. *Acta Scientiarum Naturalium Universitatis Pekinesis*, **3**, 113—117 (in Chinese).

Koo Chen-chao and Chen Yung-san, 1957: The perturbation tendency due to the dynamical disturbance of Tienshan-Altai mountains in a stratified atmosphere. *Ke Hsueh T'ung Pao (Scientia)*, no. 12, 379—380 (in Chinese).

Koo Chen-chao and Chao Ming-tza and Chih Li-jen, 1957: Tendency computations for synoptic cases showing strong dynamical disturbance by Tienshan-Altai mountain ranges. (Manuscript.)

Koo Chen-chao and Chow Shao-ping, 1957: The influence of the slope of a plateau on the movement of troughs and ridges (in preparation).

Koo Chen-chao and Yeh Tu-cheng (see reference of I and II).

Yeh Tu-cheng, Lo Szu-wie and Chu Pao-chen (see reference of (I)).

REFERENCES

BOLIN, B., and CHARNEY, J. G., 1951: Numerical tendency computation from the barotropic vorticity equation. *Tellus*, **3**, 248—257.

CHARNEY, J., 1947: The dynamics of long waves in a baroclinic westerly current. *J. Met.*, **4**, pp. 125—162.

FJØRTOFT, R., 1952: Numerical method of integrating the barotropic vorticity equation. *Tellus*, **4**, 179—194.

PALMÉN, E., 1949: On the origin and structure of high-level cyclones south of the maximum westerlies. *Tellus*, **1**, 22—31.

SAWYER, J. S., and BUSHBY, F. H., 1953: A baroclinic model-atmosphere suitable for numerical integration. *J. Met.*, **10**, 54—59.